International Journal of Bifurcation and Chaos, Vol. 13, No. 2 (2003) 505–509




# THE INVARIANT TORI FOR THE 2-MODE DAMPED, DRIVEN SINE-GORDON ODE

CHI-JER YU
*Department of Accounting,*
*Overseas Chinese Institute of Technology, Taichung 407, Taiwan*
*ycj@ocit.edu.tw*

JONG-EAO LEE
*Department of Applied Mathematics,*
*National Chiao Tung University, Hsinchu 30050, Taiwan*
*jlee@math.nctu.edu.tw*

Received January 10, 2001; Revised November 27, 2001

In this paper, we perform our algorithm developed in [Yu & Lee, 2001] to present the entire branches of quasiperiodic solutions starting from the bifurcation points in the branches of periodic solutions in an interval of parameters for the 2-mode damped, driven sine-Gordon ODE.

*Keywords*: Quasiperiodic; invariant; tori; bifurcation; numerical.

## 1. Introduction

In [Yu & Lee, 2001], we developed an algorithm to seek a new branch of quasiperiodic solutions from a Hopf bifurcation point in a branch of periodic solutions of the truncated 2-mode damped, driven sine-Gordon ODE,

$$\ddot{a}_0 + 0.04\dot{a}_0 = -\sqrt{12}J_0\left(\frac{a_1}{\sqrt{6}}\right)\sin\left(\frac{a_0}{\sqrt{12}}\right) - \Gamma\sqrt{12}\cos(0.87t)\,, \tag{1}$$

$$\ddot{a}_1 + 0.04\dot{a}_1 = -\left(\frac{2\pi}{12}\right)^2 a_1 - 2\sqrt{6}J_1\left(\frac{a_1}{\sqrt{6}}\right)\cos\left(\frac{a_0}{\sqrt{12}}\right)\,,$$

where $\Gamma$ is the parameter, and $J_0$, $J_1$ are the Bessel functions.[1] Here, for conventional reason (for example, see [Xiong, 1991]), $\omega = 0.87$, $\alpha = 0.04$, $L = 12$. Let $b_0(t) = \dot{a}_0(t)$, $b_1(t) = \dot{a}_1(t)$, then Eqs. (1) are reduced to a system of first-order nonautonomous ODEs,

[1]The $N$-mode s-G ODE is truncated from the damped, driven s-G PDE (e.g. [Xiong, 1991; Yu & Lee, 2001]),

$$\begin{cases} u_{xx} - u_{tt} = \sin u + \alpha u_t + \Gamma\cos(\omega t), \\ u(x+L,\,t) = u(x,\,t)\,, \end{cases}$$

with $u(x,\,t) = \sum_{j=0}^{N-1} a_j(t)e_j(x)$, $j = 0, \ldots, N-1$, where $e_j(x) = C_j\cos(2j\pi x/L)$, an orthonormal basis on $[-L/2,\,L/2]$.

$$\begin{bmatrix} \dot{a}_0 \\ \dot{b}_0 \\ \dot{a}_1 \\ \dot{b}_1 \end{bmatrix} = \begin{bmatrix} b_0 \\ -0.04b_0 - \sqrt{12}J_0\left(\frac{a_1}{\sqrt{6}}\right)\sin\left(\frac{a_0}{\sqrt{12}}\right) - \Gamma\sqrt{12}\cos(0.87t) \\ b_1 \\ -0.04b_1 - \left(\frac{2\pi}{12}\right)^2 a_1 - 2\sqrt{6}J_1\left(\frac{a_1}{\sqrt{6}}\right)\cos\left(\frac{a_0}{\sqrt{12}}\right) \end{bmatrix}. \tag{2}$$

In this paper, we apply our algorithm to the other Hopf bifurcation point on the same branch (as in Fig. 1, Table 1, and will be explained later). We observed that, different to those in Fig. 2 which were developed in [Yu & Lee, 2001] where the invariant curves are geometrically stable while extremely unstable in dynamics, the invariant curves in the new branch behave in totally opposite ways, i.e. they are relatively much more stable in dynamics yet their geometry is very unstable, as will be explained later.

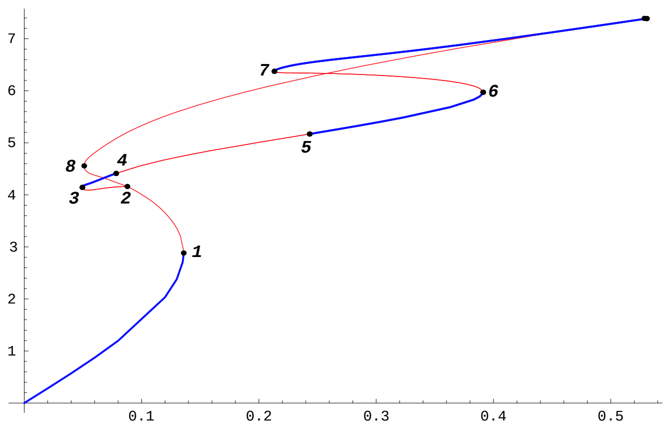


Fig. 1. The bold lines represent stable periodic orbits.

## 2. Bifurcation Diagram

The branches of periodic solutions of Eq. (2) are shown in Fig. 1 and Table 1. Each point along those branches represents a periodic orbit $f(t, \Gamma)$ where the $x$-axis is $\Gamma$ and the $y$-axis is the average norm $(1/T)\int_0^T |f(t, \Gamma)|dt$. Notice that, since Eq. (2) is nonautonomous, all periodic solutions have the same period $T = 2\pi/\omega$. At this stage, our result is identical to the result of [Xiong, 1991]. In

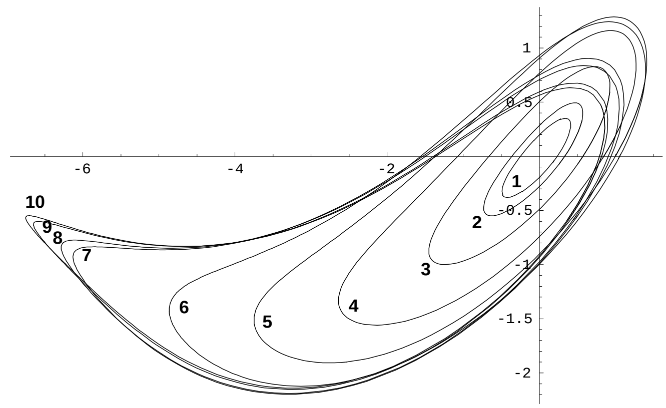


Fig. 2. Projection of invariant curves on the $(v_1, v_2)$-plane (horizontal $v_1$-direction, vertical $v_2$-direction) where $v_1 = (1, 0, 1, 0)$, $v_2 = (0, 1, 0, 1)$ with the origin $(3.0384, -2.4048, 1.8238, -1.0612)$. #2 is on a degenerate torus composed of periodic flows.

Table 1. Detailed data for the special periodic orbits in Fig. 1.

| No. | $\Gamma$ | The Point $(a_0, b_0, a_1, b_1)$ at $t = 0$ in each orbit | |
|---|---|---|---|
| 1 | 0.13576883 | $(-2.83446, -0.52587, 0.00000, 0.000000)$ | turning |
| 2 | 0.08771292 | $(-3.76470, -1.77319, 0.00000, 0.000000)$ | bifurcation |
| 3 | 0.04936938 | $(-0.35558, -3.83029, 0.04226, -1.54063)$ | turning |
| 4 | 0.07818738 | $(3.038438, -2.40477, 1.82377, -1.06116)$ | Hopf bifur. |
| 5 | 0.24312576 | $(3.609704, -0.90174, 3.56885, -0.38254)$ | Hopf bifur. |
| 6 | 0.39100055 | $(2.703455, -0.74562, 5.27208, -0.07098)$ | turning |
| 7 | 0.21305707 | $(2.406232, -1.96636, 4.82407, 2.776126)$ | turning |
| 8 | 0.05093021 | $(-0.42442, -4.53817, 0.00000, 0.000000)$ | turning |

Table 2. A list of points on each of the invariant curves in Fig. 2.

| No. | Γ | κ | One Point in Each Invariant Torus |
|---|---|---|---|
| 1 | 0.077809950131 | 6 | (3.0068369, −2.4313861, 2.0346760, −1.0915413) |
| 2 | 0.077433369764 | 7 | (2.9957650, −2.4349805, 2.1218120, −1.1066790) |
| 3 | 0.075759950131 | 7 | (3.0006727, −2.3797740, 2.3694473, −1.1546730) |
| 4 | 0.072059950131 | 7 | (3.0305030, −2.2429552, 2.6643805, −1.2396269) |
| 5 | 0.068059950131 | 8 | (3.0482276, −2.1256094, 2.8221643, −1.3305490) |
| 6 | 0.063659950131 | 9 | (3.0347579, −2.0525683, 2.8654246, −1.4388124) |
| 7 | 0.058271099694 | 13 | (2.6521675, −2.4298479, 2.6852601, −1.6141144) |
| 8 | 0.057632139695 | 14 | (2.6482699, −2.4204007, 2.6629485, −1.6285777) |
| 9 | 0.056299117535 | 18 | (2.6401067, −2.4003577, 2.6038422, −1.6565491) |
| 10 | 0.055993300836 | 20 | (2.6376785, −2.3962939, 2.5875636, −1.6623931) |



a further work, we have found two Hopf bifurcation points, namely #4 and #5 in Fig. 1.

Theoretically, there is a new branch of quasiperiodic solutions bifurcated from each of the two bifurcation points, i.e. in Poincaré sections,[2] branches of invariant curves should be born. In the following figures, those numbered and ordered curves in the Poincaré sections represent some of the quasiperiodic tori in the branch as the parameter Γ varies.

### 2.1. *Hopf bifurcation point #4*

To start and continue this new branch from the bifurcation point #4, we developed our algorithm [Yu & Lee, 2001]. As shown in Fig. 2 with detailed data in Table 2, where $\kappa$ is the maximum integer less than or equal to the reciprocal of the rotation number,[3] the tori are apparently growing with $\kappa$ increasing rapidly. But, after curve #8, those curves immediately become almost undistinguishable. This indicates that the dynamics of the system has a dramatic change for this range of parameter.

### 2.2. *Hopf bifurcation point #5*

As shown in Figs. 3–7 with detailed data in Table 3, we illustrate the new branch of the quasiperiodic solutions starting from the bifurcation point #5 in Fig. 1. Here, we found very different phenomena from that shown in Fig. 2. On one

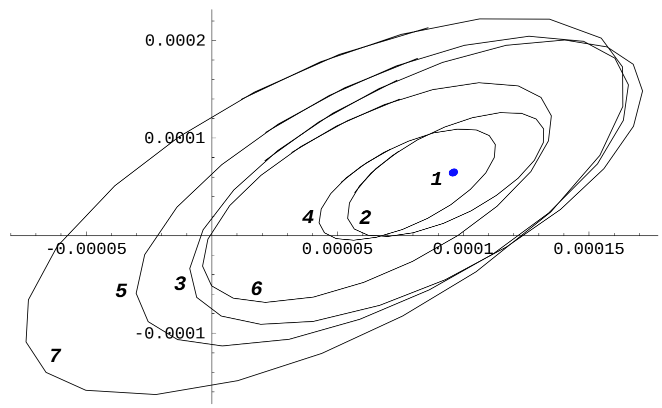


Fig. 3. Projection of invariant curves on the $(v_1, v_2)$-plane (horizontal $v_1$-direction, vertical $v_2$-direction) where $v_1 = (1, 0, 1, 0)$, $v_2 = (0, 1, 0, 1)$ with the origin (3.6097, −0.9017, 3.5688, −0.3825). Curve #1 is almost a periodic orbit.

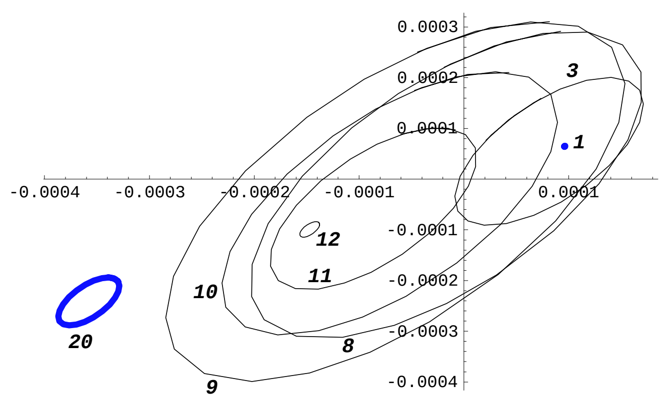


Fig. 4. Projection of invariant curves in a further variation of Γ follows Fig. 3. Curve #20 is a turning point in the whole branch.

[2]See Sec. 1.5 in [Guckenheimer & Holmes, 1993].
[3]See definition in [Guckenheimer & Holmes, 1993].

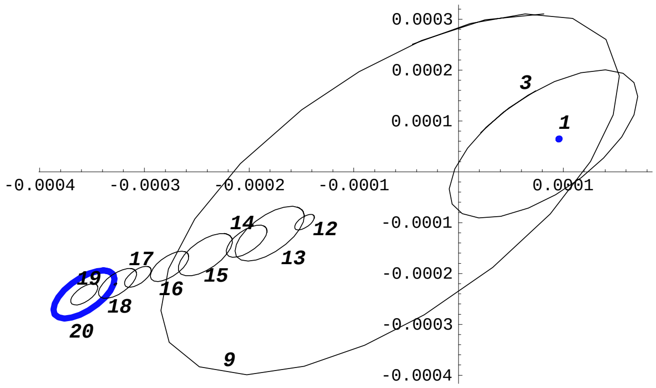


Fig. 5. Projection of invariant curves in a further variation of Γ follows Fig. 4.

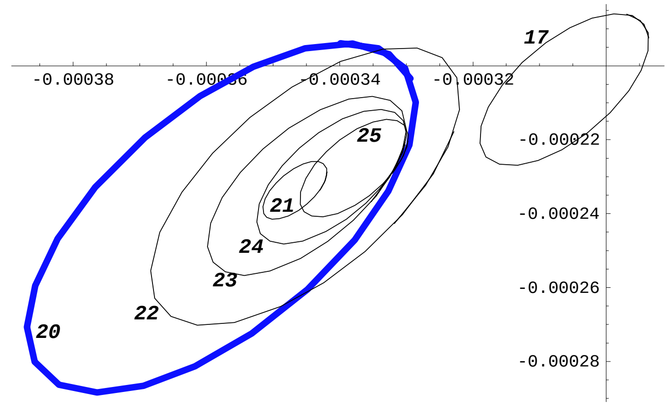


Fig. 6. Projection of invariant curves in a further variation of Γ follows Fig. 5.

Table 3. A list of points on each of the invariant curves in Figs. 3–7.

| No. | Γ | One Point in Each Invariant Torus |
|---|---|---|
| 1 | 0.243141125798 | (3.6096751, −0.90170201, 3.5689838, −0.38252321) |
| 2 | 0.243140641398 | (3.6096496, −0.90170566, 3.5689677, −0.38256568) |
| 3 | 0.243138745871 | (3.6095982, −0.90168933, 3.5689616, −0.38259390) |
| 4 | 0.243138186567 | (3.6096504, −0.90170448, 3.5689563, −0.38255728) |
| 5 | 0.243136615826 | (3.6095900, −0.90168014, 3.5689594, −0.38257971) |
| 6 | 0.243136272400 | (3.6096179, −0.90169125, 3.5689525, −0.38256699) |
| 7 | 0.243132947697 | (3.6095762, −0.90166996, 3.5689484, −0.38256794) |
| 8 | 0.243123086071 | (3.6095414, −0.90164635, 3.5689147, −0.38254192) |
| 9 | 0.243115310071 | (3.6095370, −0.90164254, 3.5688764, −0.38252480) |
| 10 | 0.243114448770 | (3.6095927, −0.90167663, 3.5688457, −0.38252724) |
| 11 | 0.243111950235 | (3.6096547, −0.90171706, 3.5688001, −0.38253275) |
| 12 | 0.243102248737 | (3.6097472, −0.90179700, 3.5686739, −0.38257608) |
| 13 | 0.243096933896 | (3.6097499, −0.90179676, 3.5686466, −0.38256203) |
| 14 | 0.243093409214 | (3.6097615, −0.90181413, 3.5686087, −0.38258036) |
| 15 | 0.243087107650 | (3.6097670, −0.90182556, 3.5685616, −0.38258808) |
| 16 | 0.243081647473 | (3.6097822, −0.90184462, 3.5685122, −0.38260189) |
| 17 | 0.243076801955 | (3.6097922, −0.90186022, 3.5684690, −0.38261598) |
| 18 | 0.243073710251 | (3.6097950, −0.90186471, 3.5684474, −0.38261701) |
| 19 | 0.243068636097 | (3.6098071, −0.90188107, 3.5684026, −0.38262938) |
| 20 | 0.243068576864 | (3.6097978, −0.90187098, 3.5684125, −0.38261834) |
| 21 | 0.243070340654 | (3.6098104, −0.90188300, 3.5684104, −0.38263255) |
| 22 | 0.243070592307 | (3.6098220, −0.90188061, 3.5684188, −0.38261166) |
| 23 | 0.243070629618 | (3.6098159, −0.90188078, 3.5684167, −0.38262045) |
| 24 | 0.243071219946 | (3.6098129, −0.90188005, 3.5684199, −0.38262387) |
| 25 | 0.243071758246 | (3.6098097, −0.90187881, 3.5684233, −0.38262638) |
| 26 | 0.243072367446 | (3.6098213, −0.90187658, 3.5684335, −0.38260637) |
| 27 | 0.243072779528 | (3.6098049, −0.90187754, 3.5684288, −0.38263181) |
| 28 | 0.243073027310 | (3.6098236, −0.90187991, 3.5684334, −0.38261228) |
| 29 | 0.243073065882 | (3.6098314, −0.90188193, 3.5684336, −0.38260641) |
| 30 | 0.243073223000 | (3.6098089, −0.90187664, 3.5684338, −0.38262500) |
| 31 | 0.243073439952 | (3.6098039, −0.90187586, 3.5684343, −0.38263030) |

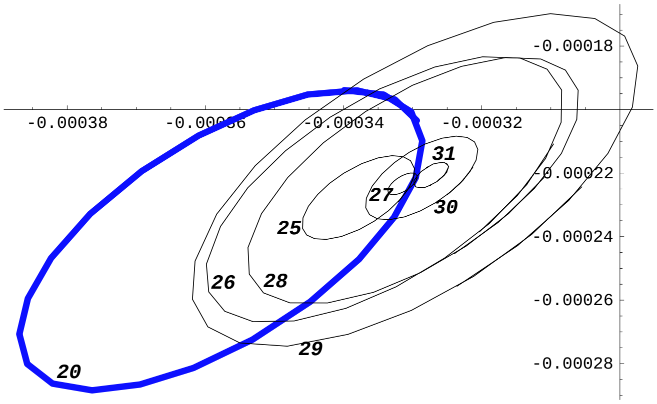


Fig. 7. Projection of invariant curves in a further variation of Γ follows Fig. 6.



hand, the dynamics of the tori are almost stable with $\kappa = 4$. On the other hand, in a very small interval of parameter, namely $0.243068576864 \leq \Gamma \leq 0.243141125798$, the geometry of those invariant curves changes rapidly in all categories such as size, shape, positions, etc. Notice that the curve #20 is a turning point in the whole branch. Indeed, due to the sensitivity in all aspects of those invariant curves, we have been extremely careful in applying our algorithm to this case.

## 3. Conclusion

Apparently, the truncated 2-mode damped, driven s-G ODE does have a complicated dynamics. The truncated 3-mode case, e.g.

$$\ddot{a}_j + \alpha \dot{a}_j = a_j \langle e_j'', e_j \rangle - \left\langle \sin\left(\sum_{i=0}^{N-1} a_i e_i\right), e_j \right\rangle - \Gamma \cos(\omega t) \langle 1, e_j \rangle\,,$$
$$j = 0, 1, \ldots, N-1\,,$$

where $N = 3$, is now under investigation. Due to the complexity of its dynamics and geometry, it is nontrivial at all to continue a smooth branch of the quasiperiodic solutions starting from a bifurcation point. We have already made some progress which is yet far from the desired result. To our knowledge, up to now, there is still no satisfactory algorithm in developing the invariant tori branch, and the reason seems quite clear. We shall continue to improve our method to do current and further research work.

## References


Guckenheimer, J. & Holmes, P. [1993] *Nonlinear Oscillations in Dynamical Systems and Bifurcations in Vector Fields*, Applied Mathematical Sciences, Vol. 42 (Springer-Verlag, NY).

McLaughlin, D. W. [1995] *Whiskered Tori for Integrable PDEs: Chaotic Behavior in Near Integrable PDEs*, Surveys in Applied Mathematics, Vol. 1 (Plenum Press, NY), pp. 83–203.

Xiong, C. [1991] "Low mode truncation method," Ph.D. thesis, Ohio State University, USA.

Yu, C.-J. & Lee, J.-E. [2001] "An algorithm to approach invariant curves," *Physica* **D149**, 30–42.